NOAA Technical Memorandum ERL FSL-1

THE LAPS SPECIFIC HUMIDITY ANALYSIS

Daniel L. Birkenheuer

Forecast Systems Laboratory
Boulder, Colorado
February 1992

noaa NATIONAL OCEANIC AND ATMOSPHERIC ADMINISTRATION / Environmental Research Laboratories

NOAA Technical Memorandum ERL FSL-1

THE LAPS SPECIFIC HUMIDITY ANALYSIS

Daniel L. Birkenheuer

Forecast Systems Laboratory
Boulder, Colorado
February 1992

NOTICE

Mention of a commercial company or product does not constitute an endorsement by the NOAA Environmental Research Laboratories. Use of information from this publication concerning proprietary products or the tests of such products for publicity or advertising purposes is not authorized.

For sale by the National Technical Information Service, 5285 Port Royal Road
Springfield, VA 22061

CONTENTS

List of Figures

THE LAPS SPECIFIC HUMIDITY ANALYSIS

Daniel L. Birkenheuer

ABSTRACT. This technical memorandum explains one aspect of the Local Analysis and Prediction System (LAPS) – the treatment of water vapor. LAPS is a collection of algorithms that has two major functions. One is to analyze atmospheric state variables from data germane to a forecast office. The second function derives fields from the state variables to help answer specific forecast questions. To date, the LAPS moisture analysis includes a cloud analysis of liquid and frozen water and a specific humidity (SH) analysis for the vapor phase. The SH analysis starting with the data sources and analysis algorithm and followed by example analyses (a clear case and one illustrating cloud treatment). Then current work and future plans of the SH analysis package are summarized. An appendix describes the horizontal shape matching (HSM) algorithm applied to this problem including the rationale used to choose the various HSM weighting coefficients. The technique to choose the HSM weighting coefficients can apply to other applications of variational analysis.

1. INTRODUCTION

1.1 Purpose

Only the status of the specific humidity (SH) analysis, one component of LAPS, is documented here. Validation of the SH analysis will be discussed in a future technical memorandum on LAPS. However, an example of the analysis product is illustrated for demonstration. The four areas of discussion are: data sources used in the analysis, a description of the algorithm, an illustration of the technique, and a summary. This report establishes a basis for future memoranda or reports concerning the development of the LAPS SH analysis procedures at the Forecast systems Laboratory (FSL).

1.2 FSL Analysis Activities

In the 1990s and beyond, local weather offices will receive increasingly more data because of advancements in automated data acquisition. For example, Doppler radar data are available only at the local weather office because their resolution and time scales pre-

vent distribution to other locations. In addition, there is no justification to convey high-resolution data of this type, indigenous to a specific locale, to another place; it can serve only the local forecast. The sheer volume of these and other data overwhelms the average forecaster. There is an immediate need to develop an analysis system to digest all perishable data in real time and deliver timely products to the forecaster that summarize the relevant facts and details indicated by all data sources. The analyses also will be used for model initialization, since advances in computer technology promise platforms capable of extensive computational sophistication at an affordable price. Such models will take advantage of local and nationally disseminated data such as satellite radiances and imagery. Many of these advanced data sets will be overlooked in a time-crunch situation unless an effective way to use them exists.

FSL is undertaking this analysis problem in its current support of the National Weather Service's (NWS) Denver AWIPS-90 Risk Reduction and Requirements Evaluation (DARE) workstation with LAPS surface analyses. Eventually, Denver NWSFO will receive the three-dimensional upper air LAPS analyses in real time.

LAPS integrates all state-of-the-art data that may be routinely available to a field forecast office. Advanced data include Doppler reflectivity and velocity fields; satellite data including Geostationary Operational Environmental Satellite (GOES) infrared (IR) dwell sounding channel data, GOES visible and IR image data, and Television Infrared Operational Satellite (TIROS) data; wind profiler data, dual-channel ground-based radiometer data, and automated aircraft reports or ACARS data, the ARINC (Aeronautical Radio, Inc.) Communication Addressing and Reporting System.

Two fundamentally different analyses are currently produced operationally at FSL: the Mesoscale Analysis and Prediction System (MAPS) and LAPS. This discussion is about LAPS, the smaller scale of the two, but since many background fields used in LAPS come from MAPS, a brief description of MAPS is prerequisite.

1.2.1 The Mesoscale Analysis and Prediction System

MAPS is a national-scale analysis with a domain covering the 48 contiguous states. Currently it operates with a 60 km grid spacing and runs every 3 hours. Its analysis scheme is optimal interpolation (OI), and its grid is orthogonal on a polar stereographic projection. Besides the analyses, forecast fields are generated at 3-h intervals out to 12 h (at 0000 UTC and 1200 UTC), and out to 6 h at other times. The vertical coordinate system for MAPS is a hybrid scheme consisting of a combination of isentropic (θ) and σ coordinates. The hybrid coordinate system renders better resolution near the surface with σ coordinates while taking advantage of the attributes of the θ coordinate system at upper levels. The data sources used in MAPS include surface and upper-air data from wind profilers and conventional rawinsondes, MAPS forecast data, and ACARS. More information about the MAPS system may be found in Benjamin (1991).

1.2.2 The Local Analysis and Prediction System

LAPS addresses local scale or meso-β scale analysis problems. LAPS is an analysis suited for local data whose large volume prohibits national operation or data support. The LAPS analysis is being developed with the understanding that products are generated from the state variable analyses for subjective forecasting and models will be initialized from the analyses.

The 10 km LAPS analysis grid nests exactly in the MAPS grid, thus MAPS analyses and forecasts are used for the LAPS background fields. The LAPS vertical coordinate system is pressure, at 50 hPa spacing, which forms 21 vertical levels from 1100 to 100 hPa. LAPS operates on an hourly cycle and uses all available data sources, most of which are asynchronous and at acquisition rates much more frequent than the analysis interval. These sources include surface aviation observations, surface mesonet, Doppler radar data, satellite data (including GOES image and dwell sounding radiance fields), wind profiler data, dual-channel microwave radiometer data (water vapor and liquid water data), and aircraft reports. Additional documentation on the LAPS system may be found in McGinley et al. (1991).

Both FSL staff and the NWSFO in Denver access LAPS and MAPS analysis output through computer workstations. Only LAPS surface data are currently accessible in Denver; however, LAPS upper air data will be distributed to that forecast office in the future.

2. DATA SOURCES

The four major inputs to the LAPS SH analysis, in order of usage, are MAPS moisture analyses (or forecasts); LAPS three-dimensional cloud and temperature analyses; LAPS surface pressure, temperature, and dew point temperature fields; and GOES dwell sounding radiance fields.

2.1 MAPS Moisture

The basis for the LAPS moisture background field is the MAPS moisture analysis. The σ coordinate system in MAPS, used at boundary levels, maintains the water vapor and other state variables more effectively in a region that can be difficult using only θ coordinates. It also presides where the two coordinate systems overlap. The θ coordinate system also more effectively analyzes phenomena in the free atmosphere because air parcels stay on these surfaces when heat is conserved. The MAPS moisture variable is condensation pressure, which represents the pressure on a θ surface where condensation would occur. The chief advantage of condensation pressure on θ coordinates is its linearity. This pressure defines the temperature of condensation (dew point temperature) in this coordinate system.

2.2 LAPS Three-Dimensional Cloud and Temperature

The LAPS cloud analysis operates hourly and uses a height grid with 42 levels. The analysis produces cloud fraction ranging from zero to one, where one represents 100% cloudiness. Data sources for the analysis are conventional surface observations of cloud base and cover, window channel data (11.2 μm infrared data from GOES), ACARS aircraft reports of clouds and icing, and radar data. An initial analysis of cloud base is

established using the surface and aircraft reports. Then a cloud top is assigned using satellite 11.2 μ m radiances and the LAPS 3-D temperature analysis. Satellite data also delineate the spatial extent of the cloud cover in the horizontal. Radar echoes place clouds in three dimensions when precipitation occurs above the analyzed cloud-base level. An expanded description of the cloud analysis may be found in McGinley and Albers (1991).

MAPS analysis and forecast temperature fields form the backgrounds for the LAPS three-dimensional temperature analysis. Interpolations between a previous MAPS analysis and a future temperature forecast synthesize a field for intervening times if a current MAPS analysis is unavailable. The temperatures near the surface are modified using LAPS surface fields. Future plans will modify the MAPS field using a mass balance scheme to derive better thermal detail from the LAPS wind analysis. More information on this analysis may be found in McGinley and Albers (1991).

2.3 LAPS Surface T, p, and T_d

The LAPS surface analysis provides three input fields: surface temperature, pressure, and dew point temperature. The analysis combines a Barnes analysis with a Laplacian minimization to smooth the resultant fields. The methods summarized here are detailed in McGinley et al. (1991).

The surface temperature analysis establishes a background using surface aviation observations, the FSL mesonet, and analyzed or forecast MAPS temperatures interpolated to 700 hPA. An analysis is made of the temperature deviations between observations and the modified MAPS 700 hPa temperatures. The MAPS temperatures are modified using a standard lapse rate, which increases the MAPS 700 hPa temperature to the elevation of the observing site and grid points. The analyzed deviation field and resulting offset values are then computed for each LAPS grid point. Modifying the MAPS 700 hPa data to correspond to the terrain elevation and computed deviation using a standard lapse rate produces surface temperature values at each grid point. Surface temperature gradient structure is then added to the surface field by using horizontal shape match-

ing (HSM), which is described in Section 3.2 and in the Appendix. The GOES 11.2 μm window channel data help infer relative ground (skin) temperature variation. This step applies only to clear regions.

The pressure analysis uses altimeter settings, a topography field, and the temperature analysis. The hydrostatic equation relates the station pressure to the station elevation and reported altimeter setting and temperature.

The dew point temperature mimics the surface temperature analysis. It transforms the surface observation to 700 hPa values and then computes a deviation field against MAPS 700 hPa dew point temperatures. The deviation field analysis is transformed back to surface dew points.

2.4 GOES Moisture Fields

2.4.1 Derivation

By far, the data providing the most spatial detail are water vapor fields derived from satellite measurements. Unfortunately, they are not available hourly. Their frequency ranges from 90 minutes to once every 2 or 3 days depending on the rapid interval scanning constraints that preclude dwell sounding ingest. GOES provides data each hour in 12 infrared spectral channels (or bands) covering the continental United States. Birkenheuer (1991) reviews the algorithm currently used for the derivation of total precipitable water (TPW) fields using the GOES and ground-based, dual-channel passive microwave radiometer data. This procedure operates quasi-operationally at FSL and is a fundamental data source for SH analysis.

To obtain an indication of three-dimensional water vapor structure, the same technique can generate layer precipitable water (LPW) fields. The method parallels the TPW method except the fields are computed layer-by-layer. A review of the technique is outlined here for background.

A physical retrieval algorithm adapted from the University of Wisconsin – Madison (Hayden, 1988) generates temperature and dew point temperature profiles from Nested Grid Model (NGM) analyses or forecast fields (used as a first guess) and GOES IR radiance data. The radiances cover a large part of the west-central United States. The reason for using radiances over a larger geographic area than needed is explained later. The sounding retrieval algorithm produces a temperature and moisture profile every 80 km in clear regions. Integrating the moisture soundings over three layers provides vertical moisture structure. The set of integrated moisture profiles and their corresponding radiances form a sample from which the coefficients are derived through regression. A solution to the following equation is desired.

$$\mathbf{Ac} = \mathbf{s}, \tag{1}$$

where $\mathbf{A}$ is an n X 12 matrix containing n observations of brightness temperatures (12 channels) from the satellite data for a given period and $\mathbf{s}$ is a vector containing the integrated LPW for a particular layer corresponding to each observation using the physical retrieval algorithm. The coefficient vector $\mathbf{c}$ for a particular layer is solved by

$$\mathbf{c} = [\mathbf{A}^t\mathbf{A}]^{-1}\ \mathbf{A}^t\mathbf{s}. \tag{2}$$

Equation (2) is solved separately for each layer using iterative refinement, providing three sets of coefficients. Coefficients are computed uniquely for each period and applied only to data of that same time.

Using a relatively large geographic area for the coefficient determination overcomes the problem of cloud obscuration because the data set is large enough to provide ample clear scenes. Furthermore, the observations also represent a statewide area that extends over widely varying terrain. This ostensibly is a data set that provides a valid representation of the air mass over the LAPS domain and is sensitive to topographical variability.

Following the solution of (2), the coefficients are applied using (1) to the 12 brightness temperatures for each field of view (FOV) over the LAPS domain. After spatial

averaging of these fields, this produces three LPW fields that provide the data to fill the LAPS grid points. To assure consistency, the three LPW grids are summed and scaled on a point-by-point basis to agree with the TPW analysis mentioned earlier. Recall that the TPW field is corrected for bias using ground-based radiometer data. Cloudy areas are flagged and do not influence the final analysis.

2.4.2 Selection of Layers

Layer selection resulted from two considerations: minimal error and meteorological application. The error measurement was the L2 norm between the computed LPW using the regression coefficients and its "raw data" counterpart from the retrieval package.

Figure 1 shows the three-dimensional plot of error as the atmosphere is partitioned in various ways. All minima in this plot define candidate partitions. Three layers were subjectively selected after examining several plots, each containing monthly data that produced consistent minima. The partition levels were 780 and 640 defining three layers: surface to 780 hPa, 780 to 640 hPa, and above 640 hPa. The surface pressure was arbitrarily assigned to be 840 hPa.

3. ALGORITHM

The algorithm can be divided into three parts: the background, the horizontal shape matching (HSM) step, and missing data strategies including quality control (QC). Figure 2 shows a flow diagram of the entire process.

3.1 Background Field

3.1.1 MAPS Condensation Pressure Converted to SH

For the LAPS background two interpolations are necessary. First, MAPS hybrid coordinate data are transformed to the LAPS pressure system. This is accomplished using a Chebyshev polynomial approximation. Second, a horizontal interpolation fills interior

points, which is facilitated by the LAPS grid nesting exactly in the MAPS grid. A bicubic two-dimensional spline interpolates horizontally to the LAPS 10 km grid.

After these steps, a three-dimensional SH field exists at LAPS resolution that is consistent with the MAPS analysis. The rest of the algorithm builds on this framework, adding information from coincident LAPS analyses of temperature, clouds, surface dew point, and finally, satellite information.

3.1.2 Alignment to other LAPS Fields

The LAPS surface dew point analysis enhances detail in the boundary layer. A boundary layer depth defined initially as 100 m (but eventually intended to be a modeled quantity) provides the limits through which the surface mixing ratio is assumed constant.

A comparison of the surface pressure to the LAPS pressure level establishes the highest pressure analyzed at each grid point. Points below the ground are flagged and excluded from the subsequent analysis. This may seem an extreme step, but it is important because the mountainous terrain in central Colorado varies extensively; within this domain, the terrain extends from 900 to 700 hPa.

Following the inclusion of the surface dew points, a three-dimensional seven-point filter smooths the SH analysis to produce continuous transitions between all levels and horizontal features. Excluded from this process are points designated as below the ground.

Internal consistency within LAPS is mandatory. A final consistency check compares the moisture analysis with the LAPS temperature and cloud analyses. The LAPS dew point temperature is computed for all levels and compared to the ambient temperature; in regions of excessive humidity the SH is reduced, averting supersaturation. This situation happens because the LAPS (here essentially MAPS) background field is much cruder than the higher resolution LAPS temperature field. The cloud comparison prevents the other extreme from occurring. Here the LAPS SH values are increased in cloudy regions so that they become saturated with respect to the LAPS temperature analysis.

This step is necessary because once again the background is cruder than LAPS; additionally, MAPS does not analyze clouds.

3.2 Horizontal Shape Matching

3.2.1 Preparation of the Gradient Field

To merge LPW structure with SH data, LPW must be scaled to SH units, even hypothetically. LPW fields are normally expressed in units of length; however, since liquid water has a density of 1 g cm^{-3}, LPW also can be expressed in units of mass per unit area. A hypothetical SH field is formulated for a level that exists at the vertical midpoint of each LPW layer. The hypothetical SH at this position can be computed from

$$\frac{LPW}{\Delta p} g\,(100) = SH \tag{3}$$

where LPW is precipitable water in units of g cm^{-2}, Δp is the pressure difference in the vertical over the layer of interest (hPa), g is the acceleration of gravity (m s^{-2}), and SH (g kg^{-1}) is the layer's average specific humidity.

Assuming that the structure in the hypothetical LPW generated SH layers can be linearly interpolated in the vertical (this is done in pressure space, which is approximately linear with respect to mass) to portray structure at intervening analyzed SH levels.

The next goal is to gauge the sensitivity of the analysis fairly with respect to both background structure and gradient structure. For this, weights were derived that satisfy a specific smoothing criterion for the background and maximize the input from the satellite gradient fields at a specific spatial wavelength. Therefore, if by chance the background contains structure on the same spatial scale as the satellite data, it is given equal influence.

3.2.2 Applying HSM

The technique used to incorporate the structure of the GOES water vapor fields into the SH analysis is HSM. HSM is attractive because it combines the gradient structure

from a source (such as satellite data) with good spatial resolution but poor accuracy, and with a background field derived from low-density but high-quality ground-based measurements (here an analysis of RAOB, and aircraft data). The smoothing is tuned to remove signals at frequencies higher than would be reasonably anticipated; these frequencies may be attributable but not limited to noise in the satellite data.

HSM is an application of variational analysis that determines a function (surface) satisfying a minimum error criterion. The criterion here has three components, smoothness, gradient structure, and background, which are regulated by coefficients α, β, and γ, respectively. Each component is not entirely satisfied, but the objective is to come as close as possible. Furthermore, the method allows control of the degree with which the different components are satisfied, emphasizing one over the other.

The HSM solution is obtained by solving the partial differential equation

$$\begin{aligned} \alpha\nabla^4\phi \; - \; \beta_x\nabla^2\phi_x \; - \; \beta_y\nabla^2\phi_y \; - \; \beta\nabla^2\phi \; + \; \gamma\phi \\ = \; -\sum_{i=1}^{3}\left[\beta_{ix}\nabla^2\phi_{ix}^g \; + \beta_{iy}\nabla^2\phi_{iy}^g \; + \beta_i\nabla^2\phi_i^g\right] \; + \; \gamma\phi' \end{aligned} \tag{4}$$

where ϕ is the desired function, ϕ_i^g is the i^{th} GOES field containing desired spatial structure, and ϕ' is the background field. The β_i terms are a function of x and y, which allows the inclusion of varying cloud cover. Also, the x and y subscripts denote partial derivatives. An explanation of the derivation of the Euler-Lagrange equation, with the mechanism used to arrive at the various weights, is detailed in the Appendix.

A simple relationship between α, β, and γ will produce the desired results. On this domain, if α is 1.11 gs^4, β is 2.01 gs^2, and γ is 1 (the units of gs stand for grid spacing, and the derivation of these values is explained in the Appendix), adequate smoothing will occur and the gradients in both the satellite and background fields will receive identical treatment at a wave number corresponding to a wavelength of 65 km. The MAPS grid resolution constrains the background to wavelengths greater than 120 - 160 km; however, the addition of LAPS temperature, surface moisture, and cloud data provide the potential for higher amounts of structure appearing in the background. The values

for α, β, and γ are only meant to be a starting point, increasing or decreasing the value of β can vary the relative strength of the gradient's effects.

The β term in the HSM equation is divided into three parts, one for each hypothetical SH level: β_1, β_2, and β_3. Their sum is constrained to 2.01 gs^2. Table 1 lists the various fractional weights applied to the precipitable water layer as it relates to each LAPS pressure level. Though HSM permits all three precipitable water layers to influence any LAPS pressure level, at this time only the two adjacent precipitable water layers are applied to each LAPS pressure level. The placement of the LAPS pressure level determines the influence of the hypothetical SH fields. Thus if a LAPS pressure level happens to coexist with a SH layer, or if it exists beneath or above the outlying SH layer, it receives 100% of its structure from that layer. Alternately, if it exactly bisects two SH layer midpoints, that pressure level receives one-half its structural input from each adjacent precipitable water level.

Table 1. GOES weighting parameters

Pressure Level (hPa)	GOES weight		
	i=1	i=2	i=3
900	1.00	0.00	0.00
850	1.00	0.00	0.00
800	1.00	0.00	0.00
750	0.42	0.58	0.00
700	0.00	1.00	0.00
650	0.00	0.82	0.18
600	0.00	0.68	0.32
550	0.00	0.52	0.48
500	0.00	0.38	0.62
450	0.00	0.23	0.77
400	0.00	0.09	0.91
350	0.00	0.00	1.00
300	0.00	0.00	1.00

3.3 Missing Data Strategies

The greatest likelihood of missing data occurs with satellite data. Typically GOES dwell sounding radiances are unavailable when the satellite is used to rapidly image severe weather or potentially severe weather-producing air masses. Unfortunately this situation occurs much of the time in the convective season. New satellite platforms promise to deliver more reliable multichannel IR data (e.g., GOES-I). Regardless, the LAPS SH analysis needs to be robust enough to tolerate the absence of entire data sources.

The analysis initially generates a background field. After this the algorithm typically waits a prescribed amount of time for the arrival of satellite data. If the interval expires without satellite data, the process continues to conclusion using the background as if it were the satellite-generated SH product. The QC consistency checks execute and the analysis output becomes available at the workstation.

If the data for the consistency checks are not available, the product is complete. Appropriate flags indicate the reduced level of error checking. The level of missing data that produces an unusable product has yet to be established. The current philosophy is that even the very smooth MAPS background is superior to nothing at all.

In the future, missing data strategies will become significant with faster update cycles. With frequently produced analyses it will be advantageous to couple the analysis to a model or previous short-range forecast or analysis field (four-dimensional data assimilation). However, the frequency of the current satellite data acquisition cycles (90 minutes at best) does not justify going to a four-dimensional approach using analyses. This is feasible only if a model runs in parallel with the analysis. Current computational limitations do not allow this.

4. EXAMPLE ANALYSIS

There are two central themes in this section. The first demonstrates the physical representation of the moisture field that this analysis provides. The second shows that

the analysis is robust and provides a reasonable output since the input data set used here is not ideal. Examples are presented in Figs. 3, 4, 5, and 6. Figure 3 shows the LPW analysis used for structure. Figure 4 compares the analysis background to the final product on each horizontal surface between and including 900 and 500 hPa. Figure 5 compares vertical cross sections that extend through the center of the domain from west to east. Finally, Fig. 6 illustrates an analyzed cloud.

To reiterate, the accuracy of the analysis has yet to be determined. The figures presented simply demonstrate the output of the algorithm at this early stage of its development. Validation of the analysis will take place later as well as testing the integrity of the analysis algorithm.

4.1 Case Selection and Circumstances

The case chosen for illustration was 1245 UTC 28 June 1991 or 0700 local daylight time. The meteorology on that day was typical of a very moist June. Thunderstorms were still common, producing ample late afternoon and evening rain. The low-level wind flow was upslope as northeast winds advected moisture from the northeast part of the domain; dry conditions existed in the mountains and the southwest part of the domain. A moisture gradient occurred along the Front Range. This moisture distribution has been observed with regularity (Birkenheuer, 1991). Storms formed near the foothills (near the center of the domain) and typically moved east to northeast, advected by the prevailing southwesterly upper-level winds. Skies on this particular morning were clear.

The analysis probably will operate under a variety of circumstances with varying amounts of input data. In general it is difficult to obtain routine multichannel IR satellite data from GOES because it is not available during rapid interval scanning operations. Typically satellite data were only available for one or two periods each day. On this day, the 1300 UTC LPW field was the only one produced.

The LAPS analysis system was also not operating perfectly. The three-dimensional temperature analysis did not function because of a software error undiscovered until

later. The LAPS cloud analysis was also inoperative. However, these are not considered major factors given the clear conditions.

Finally, the LPW satellite analyses have questionable bias. The analyses are corrected for bias in relation to the TPW analysis. The TPW analysis is produced as a separate process and uses ground-based microwave radiometer data to correct bias (Birkenheuer, 1991). Unfortunately, radiometer data were unavailable during the early summer of 1991. Therefore the analysis applied a springtime bias correction that probably elevated the measured water vapor. Fortunately, HSM ignores the absolute levels in the LPW field and reacts only to the gradient structure. This structure may have slight error given the faulty bias, but for the most part it should be reliable.

The case presented for illustration is typical of a real-life situation. Some data are present, some are present but flawed, and others are entirely absent. This case provides a reasonable rendition of the analysis performance given nominal data input.

4.2 LPW Fields

Figure 3 shows the TPW and LPW fields used in the analysis. Data were acquired at 1245 UTC. The major features are embodied in the TPW field. Moisture amounts more than 2.4 cm are located in the eastern plains of Colorado. A region with less moisture exists in the central part of the domain (1.55 cm). Another noteworthy feature is the gradient in the southeast corner of the domain. Here the water vapor level drops from 2.88 to 1.62 cm across an approximate distance of 50 km.

The three LPW fields each reflect a portion of the composite TPW field. The lowest layer field shows the low moisture region in the center of the domain and a strong moist gradient to the west where moisture values increased from 0.677 to 1.32 cm. The strong gradient is just southeast of Denver. Another feature to note is the reduced vapor amounts in the mountainous terrain to the west of Denver extending to 0.8 cm in the lowest LPW field.

The middle LPW field shows the strong gradient in the Denver vicinity oriented more north to south and located farther west than the lowest LPW field. The moisture in the low region is denoted as 0.467 cm, and the high spanning the mountains has a value of 1.24 cm. At this middle atmospheric level, it is interesting that the satellite has picked up more of a signal over the mountains than over the plains. This may be partly due to sensing high water vapor amounts in the mountainous boundary layer.

In the topmost-level LPW analysis, the gradient in the southeast corner of the domain is the most notable feature. It is stronger here than at any other level; the amount of vapor ranges from 0.880 to 0.260 cm in that corner of the domain. Features over the remainder of the domain are similar to the lower levels. Higher moisture exists in the mountainous terrain, and moderate levels are over the eastern plains. Two regions have lower amounts of water vapor along the Front Range: one has 0.389 cm and the other, farther south, has 0.387 cm.

4.3 SH Analyses

Figures 4 a-i show the result of the SH analysis obtained by incorporating the gradient structure from the LPW analysis of Fig. 3. Referring to the level weighting in Table 1, Figs. 4 a-c received most of the structure from the lowest LPW field, the structure in Fig. 4 d is roughly shared equally between the lowest and middle LPW field, the structure in Figs. 4 e-g is primarily from the middle LPW analysis, and the 550 hPa field Fig. 4 i receives its structure from both the topmost and middle LPW fields. Topographical effects are evident in Figs. 4 a-e. SH values below the terrain boundary received a value of 0.0. At 700 hPa only the mountain peaks penetrate that pressure surface.

The only way to observe the effects of the increased structure introduced by the analysis is to compare these fields with their corresponding initial backgrounds, Figs. 4 j-r.

Beginning with the lowest level (900 hPa), we see that the SH analysis had little effect other than removing the gradient near the topography edge in the center of the domain. This is probably the result of the Laplacian minimization, or smoothing in the solution of the Euler-Lagrange equation. Some new structure was added in the eastern plains.

At 850 hPa a similar smoothing effect is apparent near the topographical boundary, but this also may be the effect of the analysis trying to adjust to the north-south gradient found in the LPW field used for gradient structure. This gradient is orthogonal to the one in the 850 hPa background analysis. Higher moisture values were added in the extreme eastern part of the domain.

At 800 hPa, much LPW structure is evident. The low moisture area southeast of Denver is now actually contoured, and the high amounts of moisture analyzed in the extreme northeast part of the domain emerge.

The 750 hPa field receives its structure from both the lowest LPW and the middle LPW fields. Again, greater water vapor levels are analyzed in the extreme eastern part of the domain and an added minimum contour is over east Denver, extending south. This is driven by a similar feature in the low and middle LPW fields.

At 700 hPa, the analysis appears to have decreased the water vapor in the southeast high, lowering its value from 6.16 g kg^{-1} in the background to 5.93 g kg^{-1} in the analysis. This is probably due to the minimum between the two contoured "highs" in the middle LPW field; the one to the north was 0.764 cm and the one to the south was 0.748 cm. The low near Denver is still maintained.

The 650 hPa field shows the extension of the high moisture "ridge" in the middle-level LPW field extending from the northeast corner of the domain south and then eastward. At this level we see similar contours in both the satellite and SH fields. No major differences are apparent at 600 hPa. The contours generally make more "wiggles," but there is no genuine difference in the overall representation of the moisture.

At 550 hPa, the analysis is influenced by both the middle and the highest LPW fields. Here a low is indicated (1.41 g kg^{-1}) in the southeast portion of the domain. This is probably the result of the gradient just east of the 0.88 cm high denoted in the top-level LPW field. This gradient generates the low in the SH field and a closed contour high (not labeled) to its east.

At 500 hPa, the low in the background field (0.976 g kg^{-1}) is replaced by a high at 1.17 g kg^{-1}. Just south of this high is a low. It is interesting that the gradient in the extreme southeast part of the domain exists in both the background and the top-level analysis. This goes unchanged in the final analysis. Again, there is good correspondence between the LPW field and 500 hPa structure.

4.4 Cross-Section Plots

Figure 5 shows the background and analyzed cross sections of the SH field. The cross section extends west to east through Boulder (40° north latitude). The topography is blackened. The contour lines greater than 10 g kg^{-1} were not plotted. General features between the background and analysis are roughly the same. The background is not as smooth as the final analysis. The analysis contains more "wavy" lines, especially at high levels, signifying added structure at those levels. At low levels, the 10 g kg^{-1} contour extends above 2 km in the extreme east edge. Other than this change, the low-level structure has been smoothed by the analysis; this is especially evident near the terrain.

The application of the analysis establishes the technique's ability to incorporate satellite gradient information while preserving the background "framework" acquired from MAPS and LAPS upper air and surface dew point temperature data/analyses. We see that it does this effectively; not demonstrated here is the handling of clouds. Presenting a cloud-free example helps focus on the treatment of gradient information. When clouds are included in the analysis, there are regions within the domain that do not become a part of the Euler-Lagrange solution.

To illustrate cloud effects, Fig. 6 shows the case of 25 June 1991 0900 UTC (0030 local daylight time). In this vertical cross section, the cloud is east of the mountains near the edge of the domain at 5 km altitude. The SH near the cloud is about 2 g kg^{-1}. The scheme used to assign humidity based on the presence of cloud saturated the region denoted as cloudy. This method of saturating cloudy areas can lead to very abrupt boundaries as noted by Wolcott and Warner 1989. Such boundaries may or may not represent the moisture environment. Recently, Radke and Hobbs (1991) measured humidities near clouds and they note that there can be both abrupt and gradual changes in the moisture at the cloud edge. We hope that the environmental distribution of moisture around clouds can be parameterized against cloud type or IR radiative properties of clouds. This aspect of the SH analysis remains under development.

Some candidate parameterizations include different treatments for clouds formed through convection, radiational cooling, and synoptic-scale air mass motions. Convective clouds may receive a lower degree of saturation than other clouds or fog because convection may entrain dry air effectively lowering the bulk moisture concentration. It is important to remember that though the analysis is preformed at relatively high resolution (at least compared to conventional analyses), the 10 km grid spacing is still crude on most cloud scales.

5. CONCLUSION

As stated in the introduction, the specific humidity analysis is incomplete. LAPS development eventually will improve the technique, and an analysis system will emerge that will keep pace with the demands placed on it by future models. In the short term, several areas require immediate attention: improving the boundary layer definition and interactions, resolving cloud/RH implications, establishing feedback to other LAPS analyses, and upgrading the quality control.

A better boundary layer needs to be established to allow realistic vertical distribution of surface moisture. Modeling surface fluxes of heat and humidity relating to surface type and ground moisture enable the establishment of moisture sources. Currently

only in-situ observed moisture is analyzed. This is true for both LAPS and MAPS; however, MAPS does account for vapor removal through precipitation. Moisture fields evolve so quickly that by relying only on observation, the analyst will continually be playing catch-up, never reaching an accurate real-time description of moisture distribution or phase. Clouds continue to pose problems. Currently they are inserted into the analysis with a parameterization scheme to adjust the relative humidity to suit a category of cloud type. The most suitable parameterization has yet to be established. The scheme can be made to fit an improved treatment of the cloud environment at any time.

Cloud parameterization/modeling may at some point feed back into the temperature analysis. If a cloud forms by radiational cooling, and it can be accurately located through satellite data or other means, it is possible to infer the lower temperatures that must exist in the cloudy regions. Provided the moisture characteristics of the air mass enveloping the cloud are known from prior analysis or model forecasts. In the same manner that the moisture analysis utilizes other LAPS data fields, the SH analysis could lead to modification of others such as temperature.

Improved quality control is always necessary. The current technique applies only rudimentary consistency checks. Improved quality control will come from a better understanding of physical interactions. This will be added as the analysis evolves. An obvious place for future work is in the area of four-dimensional data assimilation, either through direct coupling to previous analyses or through a model. This will be forthcoming as required.

Future work must concentrate on validation of the SH fields. The analysis is new and constantly undergoing changes, however, it is likely that when this memorandum is published, the algorithm will have changed. Validation should commence when the analysis is stable over a long period.

6. REFERENCES

Benjamin, S.G., 1991: Short-range forecasts from a 3-h isentropic-sigma assimilation system using ACARS data. *Fourth AMS International Conference on Aviation Weather Systems*, 24-26 June 1991 Paris, France. 329-334.

Birkenheuer, D., 1991: An algorithm for operational water vapor analyses integrating GOES and dual-channel microwave radiometer data on the local scale. *J. Appl. Meteor.* **30**, 834-843.

Hayden, C.M., 1988: GOES-VAS simultaneous temperature-moisture retrieval algorithm. *J. Appl. Meteor.*, **27**, 705-733.

McGinley, J.A., and S.C. Albers 1991: Validation of liquid cloud water forecasts from the Smith-Feddes method derived from soundings and LAPS analyses. *Fourth AMS International Conference on Aviation Weather Systems*, 24-26 June 1991, Paris, France, 228-233.

McGinley, J.A., S. Albers and P. Stamus, 1991: Validation of a composite convective index as defined by a real time local analysis system. *Wea. Forecasting*, **6**, 337-356.

Radke, L.F., P.V. Hobbs, 1991: Humidity and particle fields around some small cumulus clouds, *J. Appl. Meteor.*, **48**, 1190-1193.

Wolcott, S.W. and T.T. Warner, 1981: A moisture analysis procedure utilizing surface and satellite data. *Mon. Wea. Rev.*, **109**, 1989-1998.

APPENDIX

Evaluation of HSM on the LAPS grid

We derive the form of the HSM equation used in the main text, and show the derivation of the weighting coefficients for α, β, and γ.

To perform the HSM analysis, we minimize functional J:

$$J = \int\int \alpha(\nabla^2\phi)^2 + \sum_{i=1}^{3}\Big[\beta_i(\phi_x - \phi_{ix}^g)^2 \; + \; \beta_i(\phi_y - \phi_{iy}^g)^2 \;\Big] + \; \gamma(\phi - \phi')^2 \; dx \; dy, \quad \text{(A.1)}$$

where ϕ is the desired function, ϕ_i^g is the i^{th} GOES field containing desired spatial structure, and ϕ' is the background field. The terms α, β_i, and γ weight the response of the Laplacian (smoothing), gradient structure, and background, respectively. The x and y subscripts denote partial derivatives. Note that the β_i term is a function of x and y; this is because the β_i terms depend on cloud cover. We also designate $\beta = \sum_{i=1}^{3}\beta_i$. Values for β range from a maximum down to 0 in cloudy areas. One should think of this in terms of a constant β modulated by a spatially varying cloud fraction (ψ); $\psi = 1$ represents perfectly clear conditions and $\psi = 0$ represents total cloudiness. This approach assures that the analysis excludes gradient information in cloudy regions. In these regions, the background field dominates the analyzed product.

The partial differential equation satisfying the minimization can be identified using variational calculus; it is termed the Euler-Lagrange function.

$$\begin{aligned} \alpha\nabla^4\phi \; - \; \beta_x\nabla^2\phi_x \; - \; \beta_y\nabla^2\phi_y \; - \; \beta\nabla^2\phi \; + \; \gamma\phi & \\ = \; -\sum_{i=1}^{3}\Big[\beta_{ix}\nabla^2\phi_{ix}^g \; + \beta_{iy}\nabla^2\phi_{iy}^g \; + \beta_i\nabla^2\phi_i^g\Big] \; + \; \gamma\phi'. & \end{aligned} \quad \text{(A.2)}$$

This equation can be solved numerically using relaxation techniques. Now we examine the values for the weights.

To examine the effect of the Laplacian only, the β in (A.1) can be zeroed out, leaving only the α and γ terms. The resulting Euler-Lagrange equation is a simplified ver-

sion of (A.2).

$$\alpha \nabla^4 \phi + \gamma \phi = \gamma \phi' \tag{A.3}$$

The filter response of this equation can be derived by applying it to standing waves in two dimensions. Let

$$\phi = A e^{i(kx+py)} \tag{A.4}$$

and

$$\phi' = B e^{i(kx+py)}, \tag{A.5}$$

where k and p are the wave numbers in the x and y dimensions, respectively. Substituting (A.4) and (A.5) into (A.3) and evaluating gives

$$\alpha A(k^2 + p^2)^2 + \gamma A = \gamma B \tag{A.6}$$

after dividing through by $e^{i(kx+py)}$.

The expression can be reduced to one-dimensional form by introducing a wave number n such that $n^2 = k^2 + p^2$. The ratio (r) of the analyzed wave amplitude A over the input amplitude B becomes

$$r = \left[1 + \frac{\alpha n^4}{\gamma}\right]^{-1} \tag{A.7}$$

after substituting n into (A.6). It is common practice to assume a cutoff response when $r = 0.5$. GOES-derived precipitable water fields have an intrinsic spatial resolution of about 30 - 40 km. Therefore, GOES resolves a wavelength of 65 km. Given that the LAPS domain has 10 km grid spacing, the GOES information has a characteristic wave number of $2\pi/65$ km^{-1} or $2\pi/6.5$ gs^{-1}, where gs denotes grid point spacing. This is about 0.873 gs^{-1}. Assuming r is 0.5 establishes a ratio of $\frac{\alpha}{\gamma}$ equal to 1.11 gs^4.

This last exercise illustrates the performance of (A.3) in smoothing the background field; the degree of smoothing is dependent only on the ratio of the two weights for the Laplacian/biharmonic term and the background. Equation A.7 also shows that wave numbers less than the cutoff receive less attenuation (r increases to unity as n decreases to zero). This is the desired response since background information with longer wavelengths is deemed more reliable.

By applying HSM we insert the gradient structure in a way that does not detract from the background accuracy. To study the effects of the various weights we examine the clear case. Here β is constant and its derivatives are zero. Equation A.2 simplifies to

$$\alpha\nabla^4\phi \; - \; \beta\nabla^2\phi \; + \; \gamma\phi \; = \; -\sum_{i=1}^{3} \beta_i \nabla^2 \phi_i^g \; + \; \gamma\phi'. \tag{A.8}$$

The response of (A.8) can be determined in the same manner as (A.3). Letting (A.4) represent the solution and (A.5) the gradient field [transform ϕ' to ϕ_i^g in (A.5)], the response, A/B, becomes

$$r = \frac{\beta n^2}{\alpha n^4 + \beta n^2 + \gamma}. \tag{A.9}$$

With α equal to 1.11 gs^4 and γ equal to 1, β can be solved as 2.01 gs^2 (when $r = 0.5$ and $n = 2\pi/6.5\ \text{gs}^{-1}$).

Taking the derivative of (A.9) with respect to n and solving for the maximum also shows that the gradient response peaks at this wave number (6.5 gs). The gradient term produces the desired response, allowing GOES data to have maximum influence at the wave number of its highest information content. At longer wavelengths, the background field dominates since (A.7) shows that it will not be attenuated, and the gradient response goes to zero in (A.9). Both the background and the gradient waves are suppressed at wavelengths shorter than the "cutoff."

Another way to examine solutions of (A.8) is through Fourier analysis. This method also verified the HSM algorithm's computer code before operational use. Input fields are two orthogonal standing waves with equal wave number (Fig. 7). Waves in one dimension represent the background and those in the other dimension depict the GOES field. Fourier analyses of the output determine the effect of the coefficients by showing relative amplitudes of each orthogonal component. Figure 8 shows the solution and Fig. 9 shows its transformed counterpart with the applied weights 1.11, 2.01, and 1.0 (for α, β, and γ, respectively). To determine the values of a specific single-layer β_i, one must refer to Table 1, which shows the fraction of influence each layer contributes to the total structure. For testing, β was distributed to the same function at three layers, two layers, and

a single layer; all results were identical proving that the gradient structure was linearly combined. In practice, only two LPW layers interpolate the structure of a single specific humidity surface.

Shown here are the relationships between the background and gradient parts of the HSM analysis. We see that a straightforward method exists to determine the filter cut-off (effective smoothing) based on the desired spatial signal. The Fourier transformation was also effective in verifying the performance of the HSM filtering characteristics. Modifications of this HSM method potentially have wide application. Similar approaches to the assignment of weighting coefficients in those other applications may prove useful.

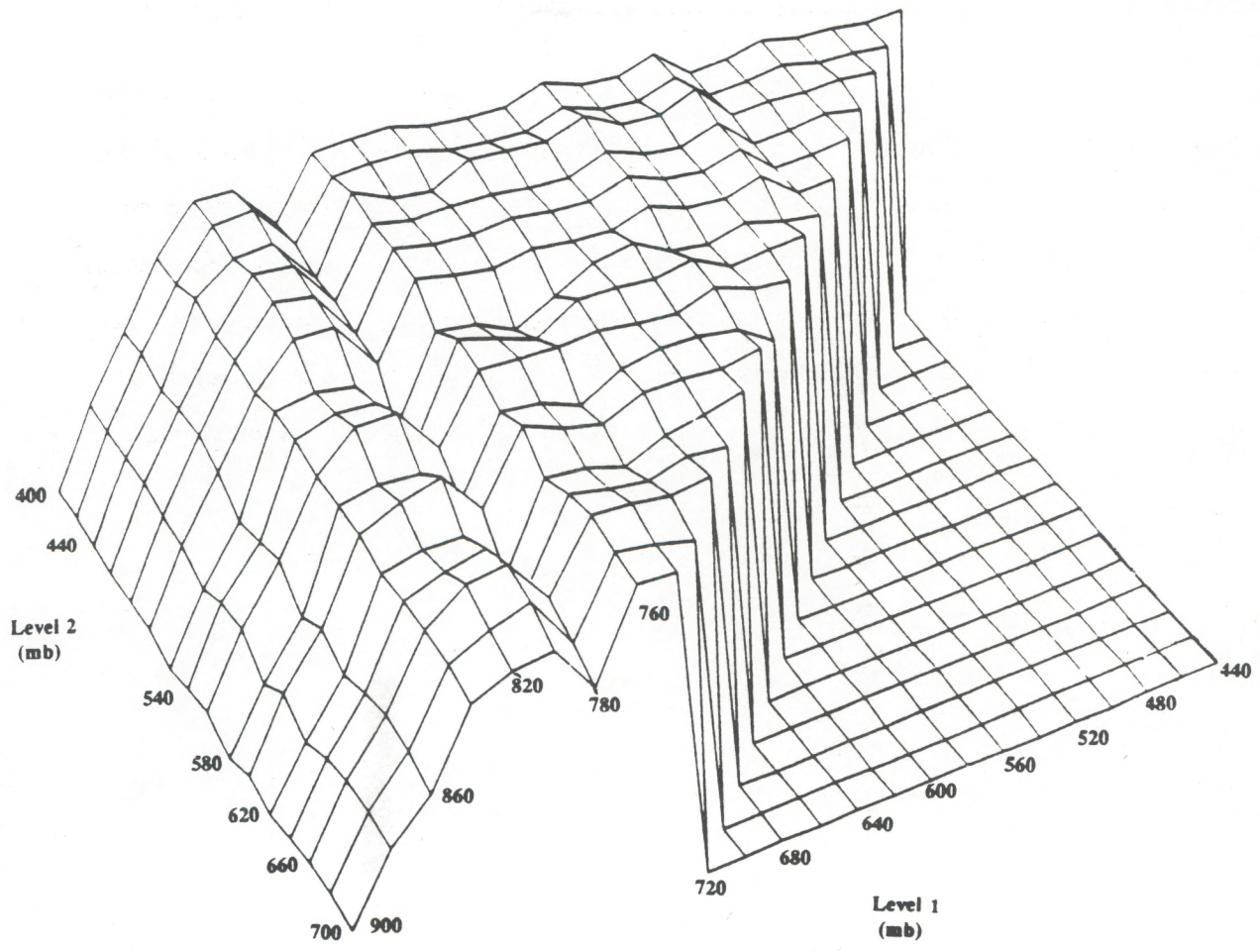

Fig. 1. Three-dimensional plot of residual error vs. partition levels. Minima in this surface are all candidates for defining two atmospheric partitions. Regions near the plot boundaries were not considered since averages in these areas may be unrepresentative due to decreased sample size.

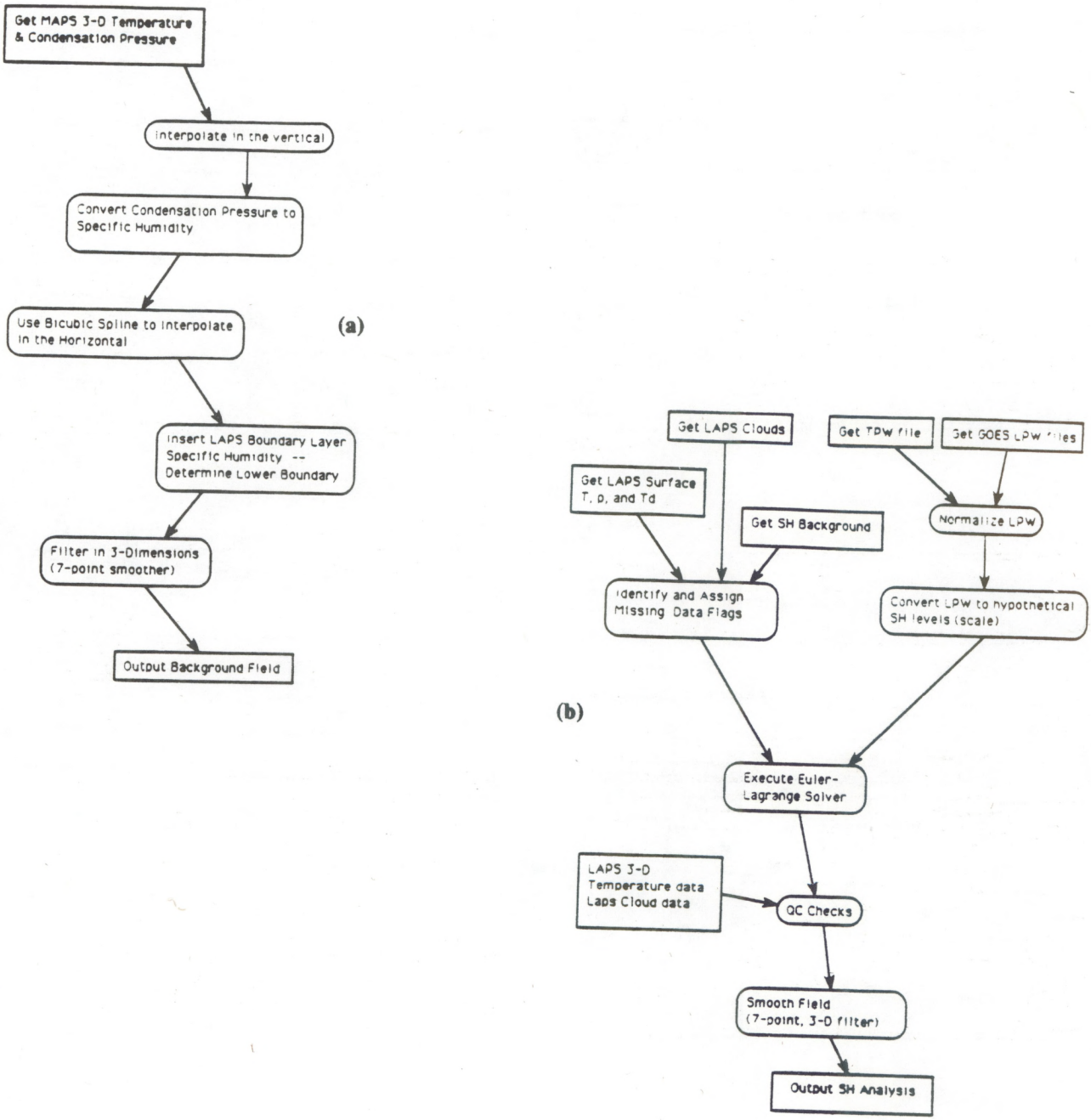

Fig. 2. Flow charts of current analysis algorithm: (a) the first step in the procedure generating SH background field and (b) the second step combining the background with LPW gradient information through HSM. Both procedures produce output files that include information on the boundary layer surface dewpoint temperature.

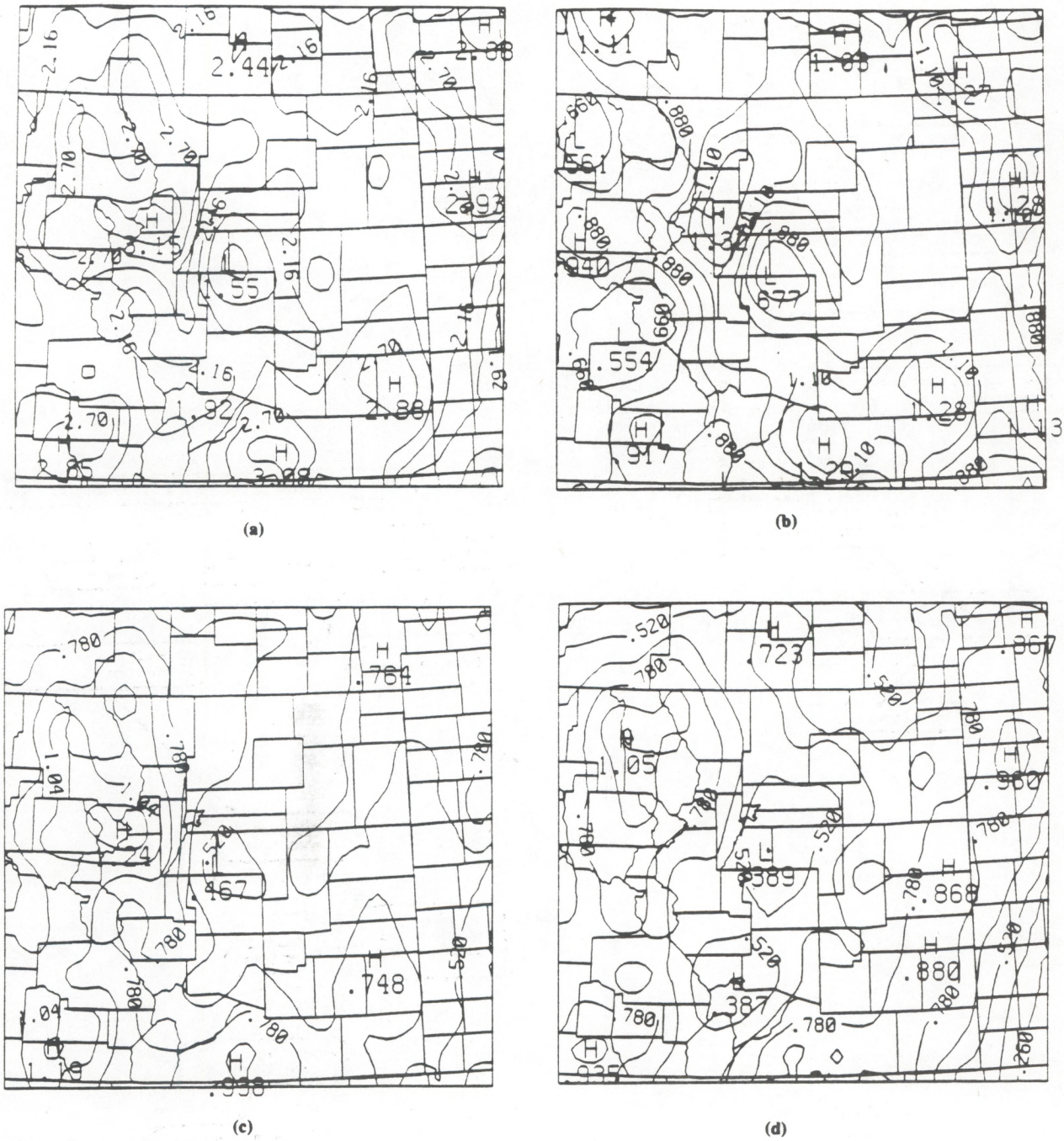

Fig. 3. Precipitable water background fields (in centimeters) for 1245 UTC 28 June 1991: (a) total precipitable water field derived using the method described in Birkenheuer (1991); (b) lowest-level LPW field, depicting moisture from surface to 780 hPa; (c) middle-level LPW field, representing 780 to 640 hPa; and (d) topmost-level LPW field contouring moisture above 640 hPa.

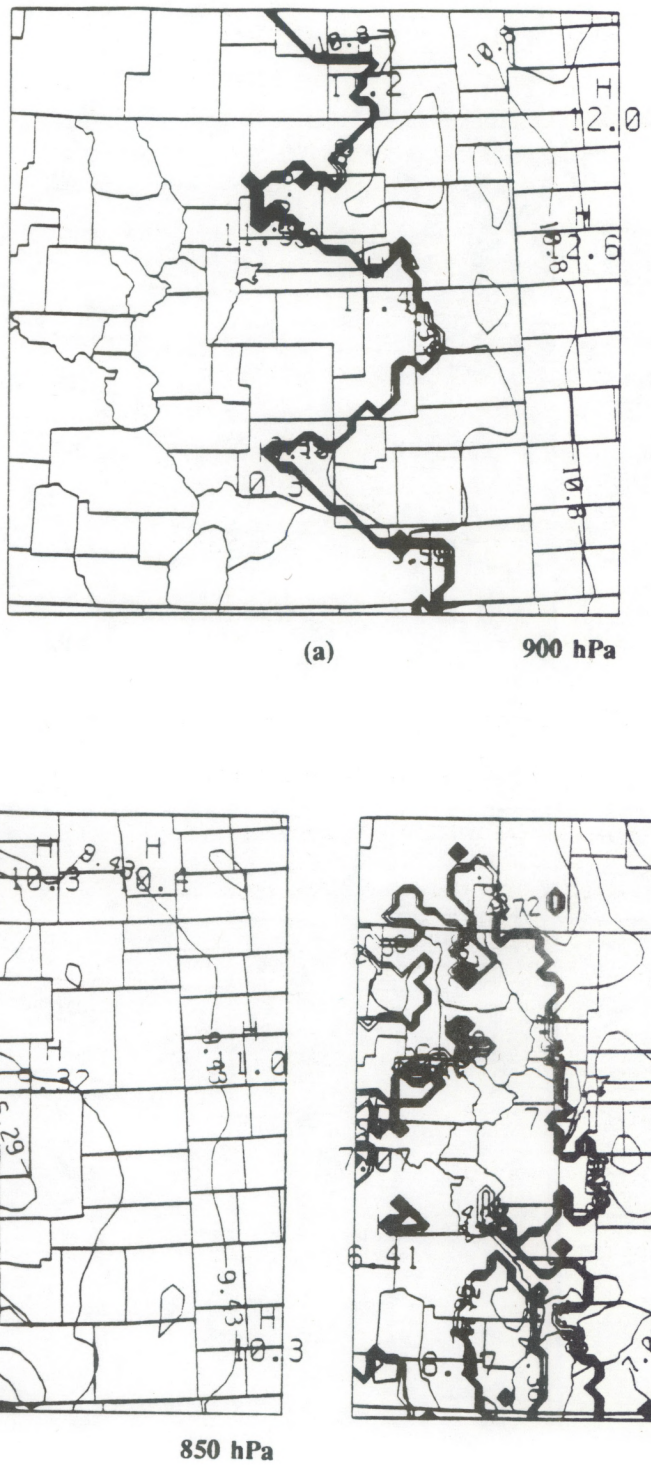

Fig. 4. Series of (a-i) SH analyses ranging from 900 to 500 hPa and (j-r) corresponding background fields 1300 UTC 28 June 1991.

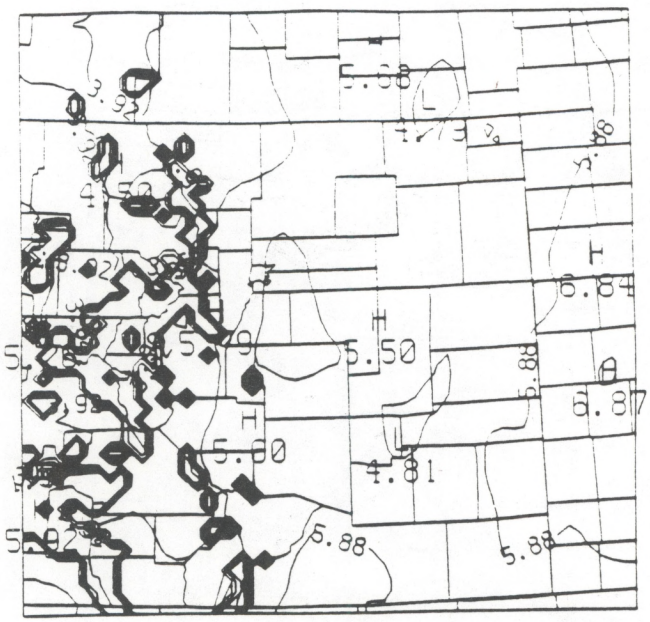

750 hPa

(4d)

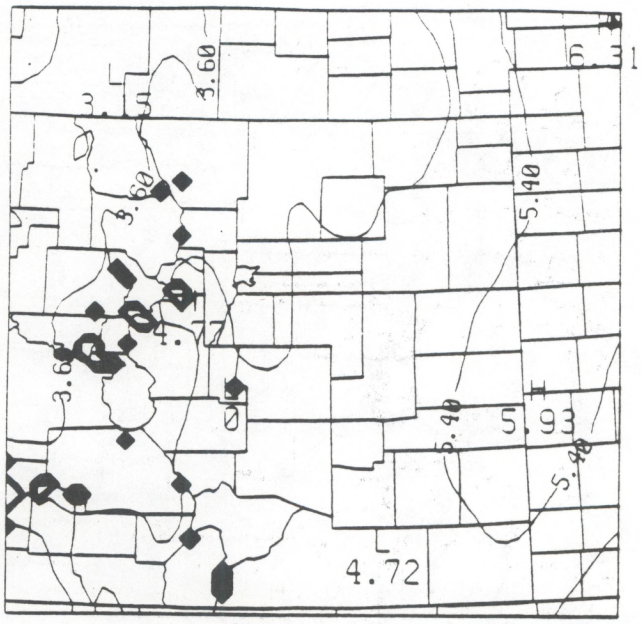

700 hPa

(4e)

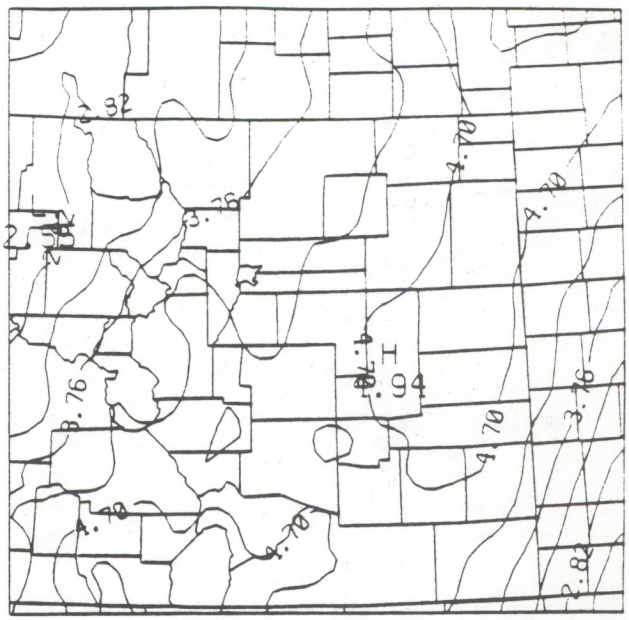

650 hPa

(4f)

Fig. 4 (continued)

600 hPa

(4g)

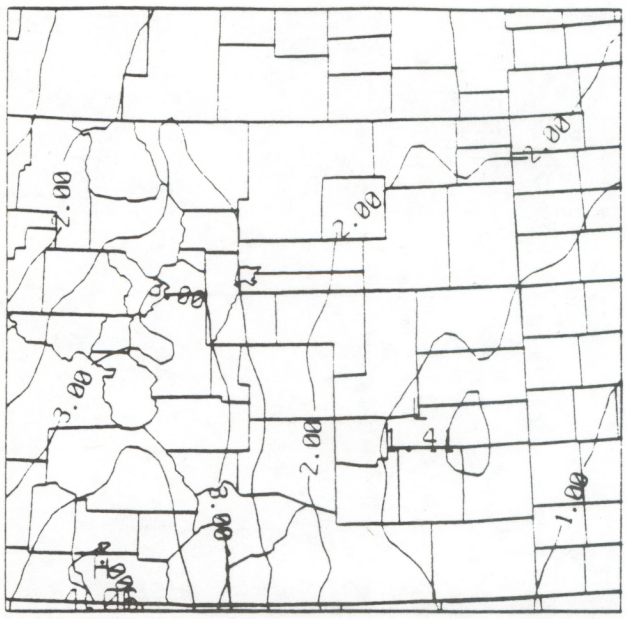

550 hPa

(4h)

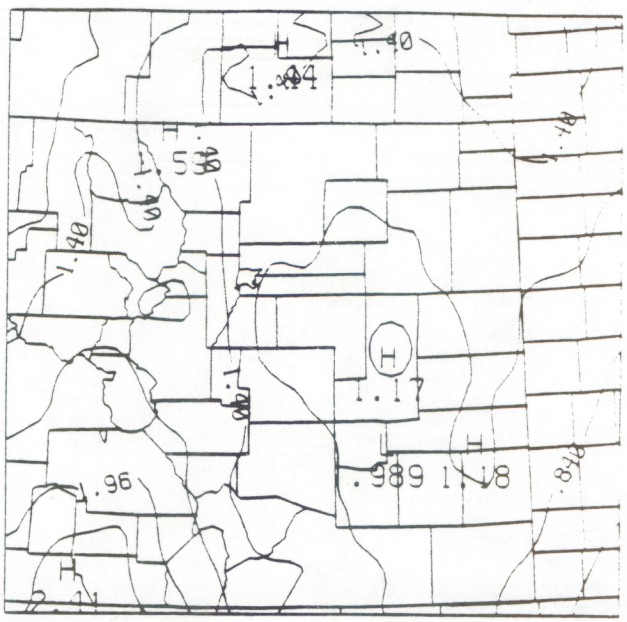

(4i)

500 hPa

Fig. 4 (continued)

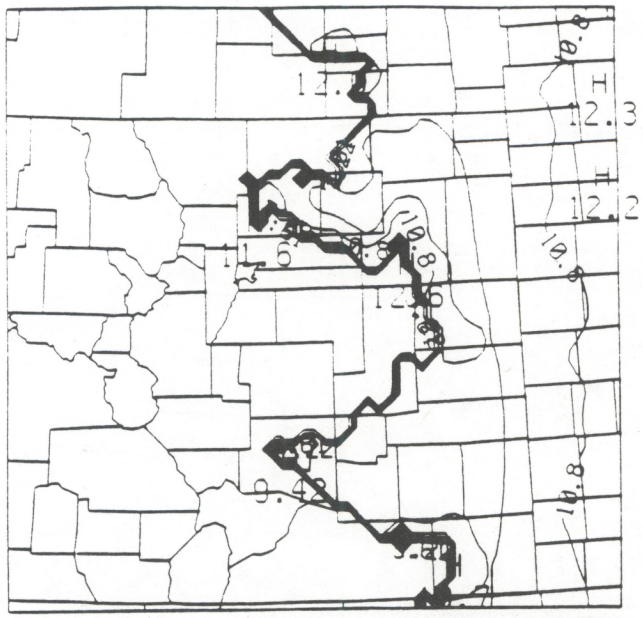

(4j) 900 hPa

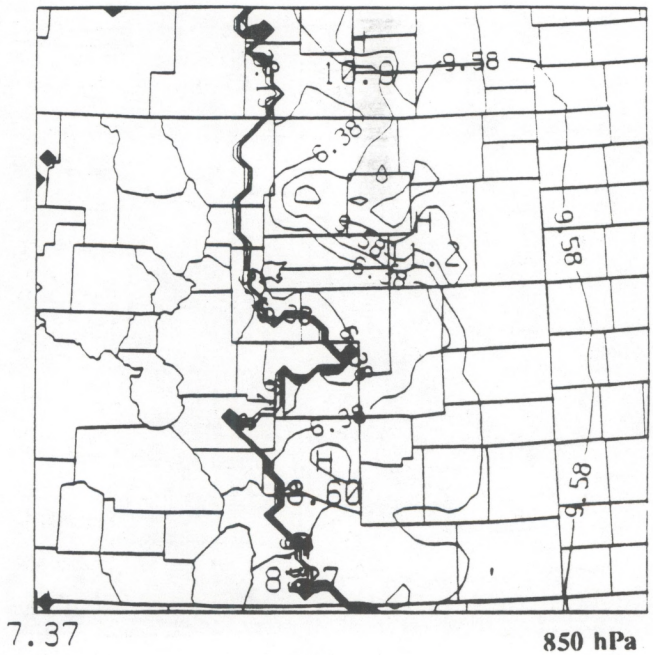

(4k) 850 hPa

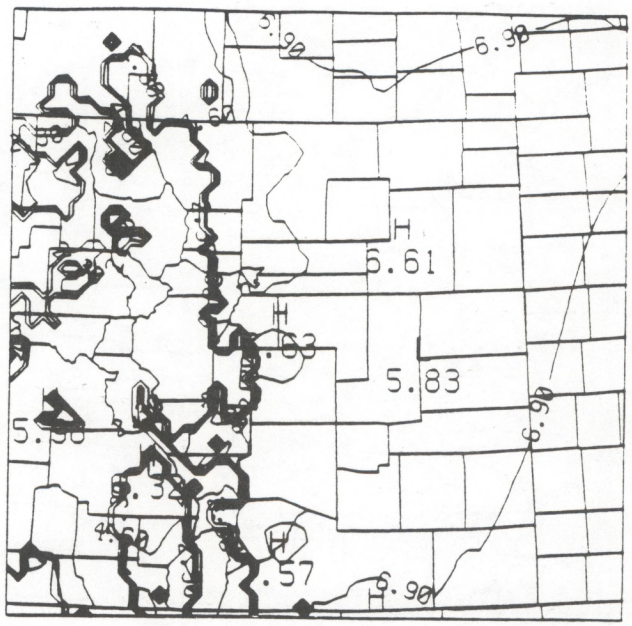

(4l) 800 hPa

Fig. 4 (continued)

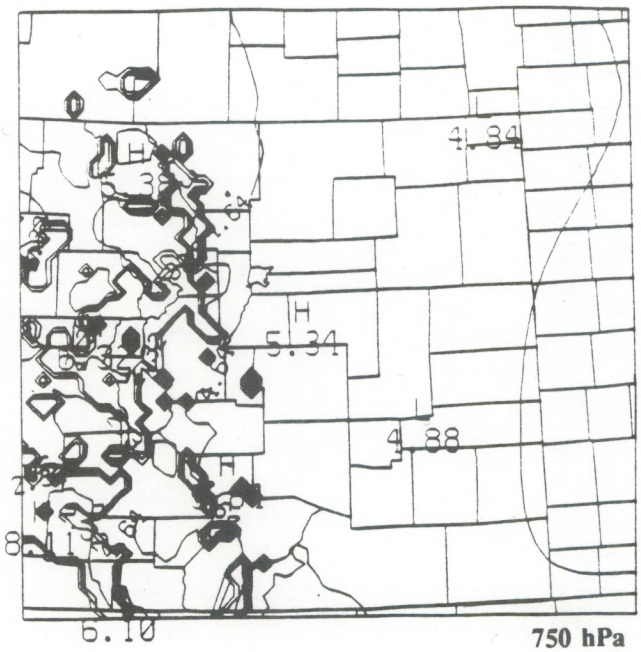

750 hPa

(4m)

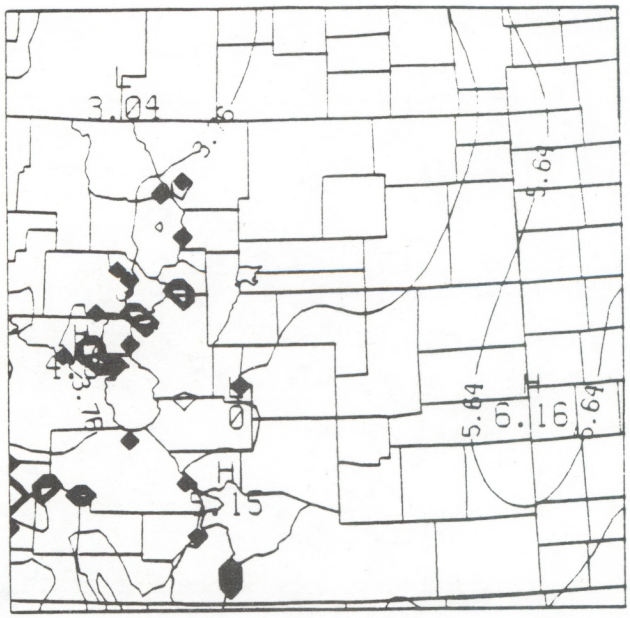

(4n)

700 hPa

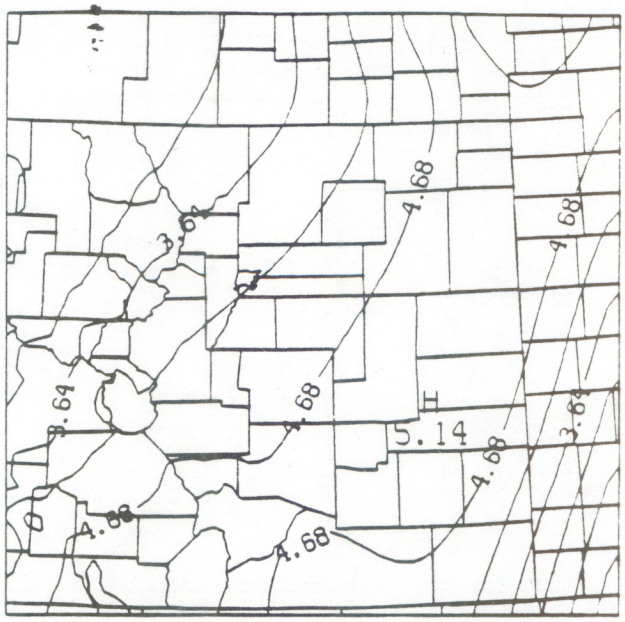

650 hPa

(4o)

Fig. 4 (continued)

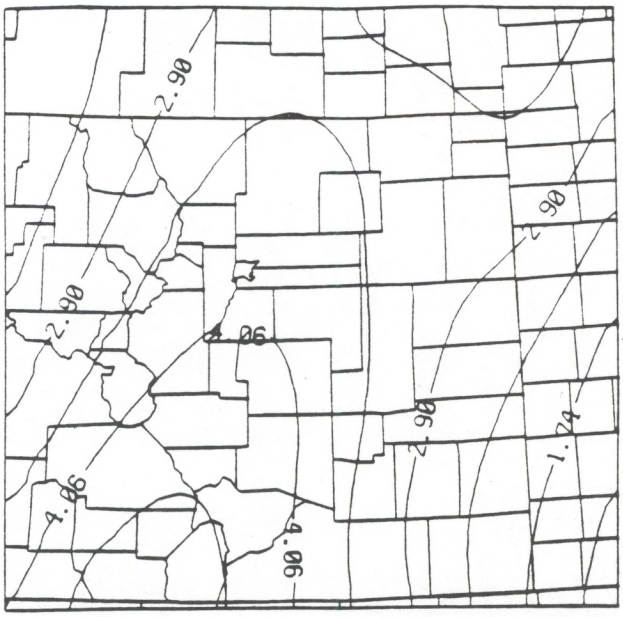

600 hPa

(4p)

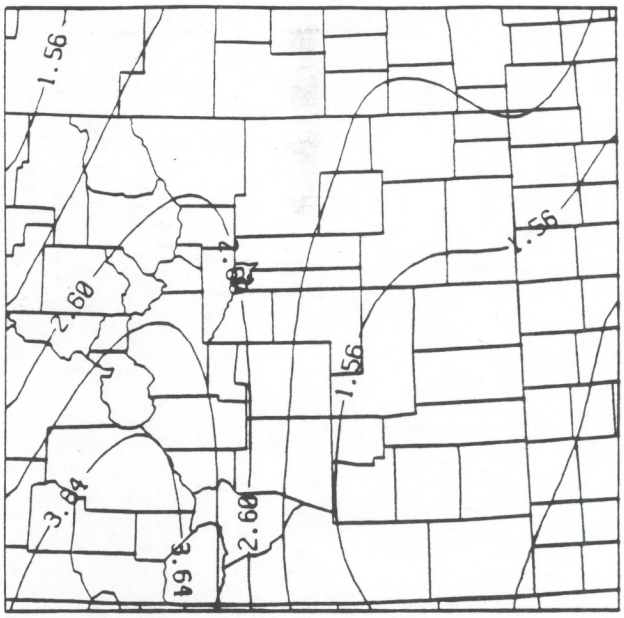

550 hPa

(4q)

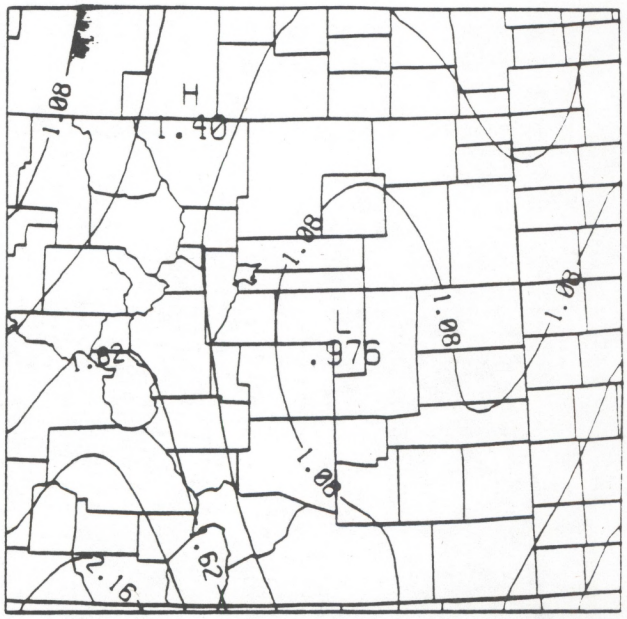

500 hPa

(4r)

Fig. 4 (continued)

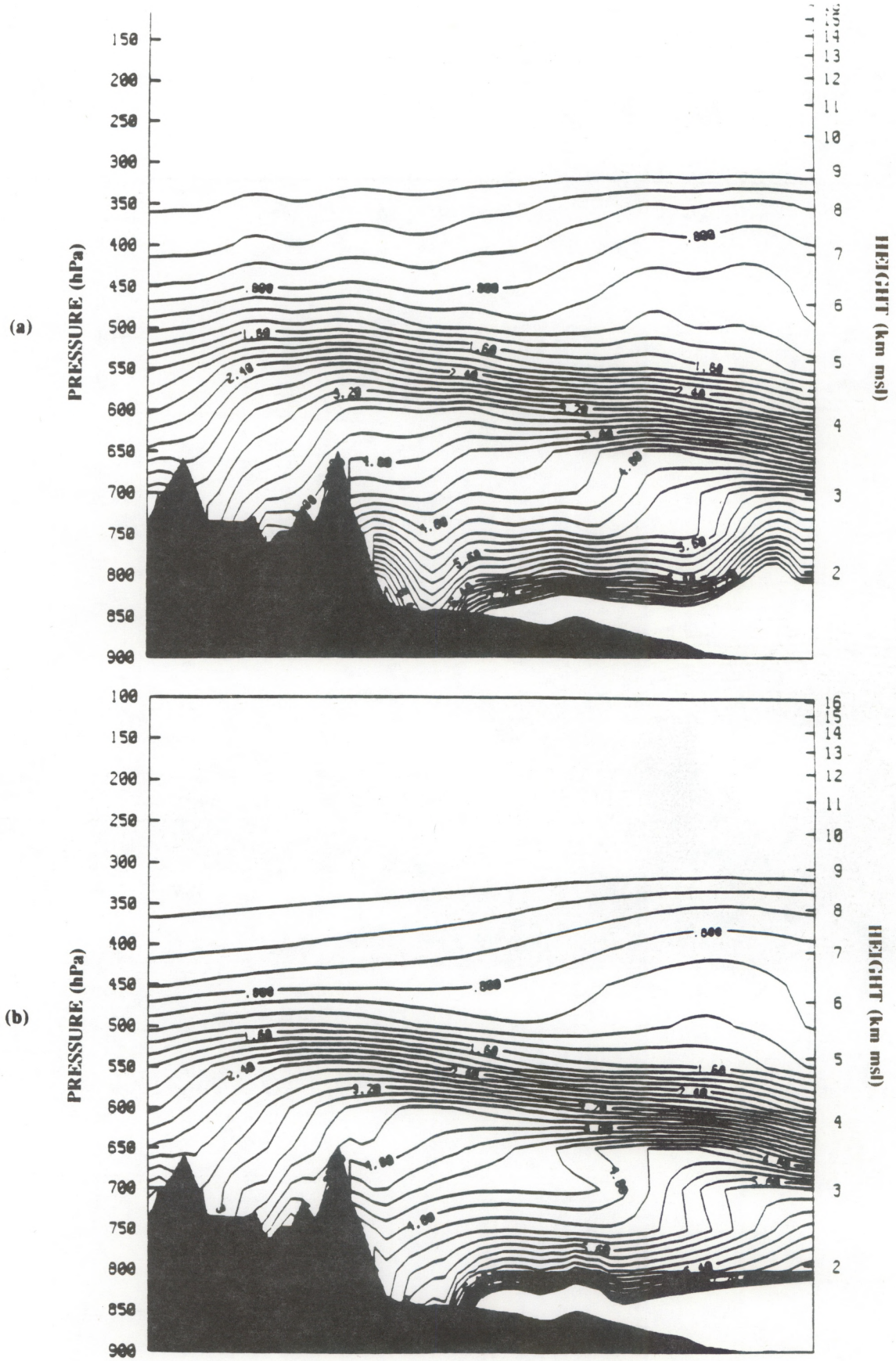

Fig. 5. Cross section of (a) analysis and (b) background fields for 1300 UTC 28 June 1991.

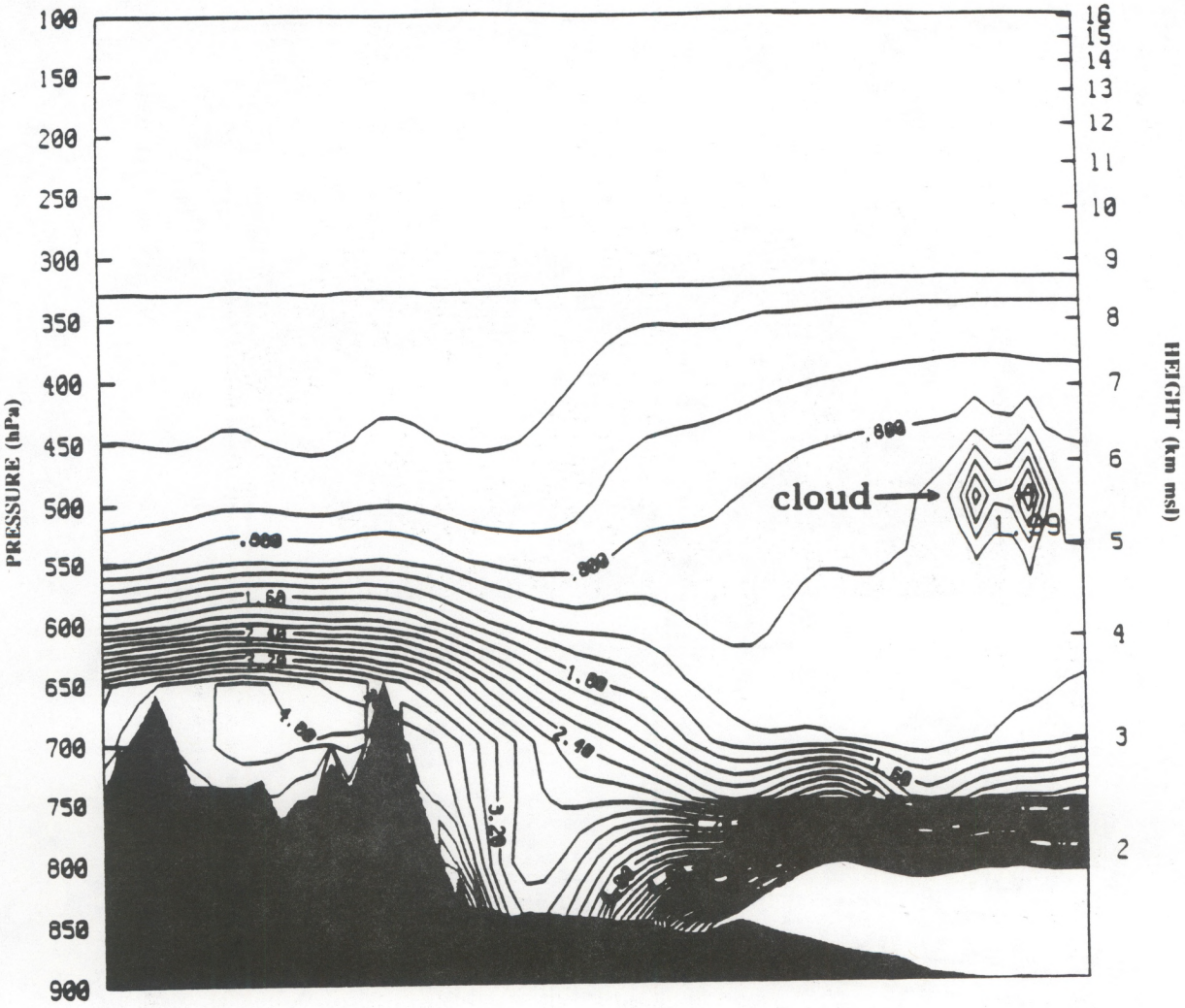

Fig. 6. Cross section showing presence of a cloud for 0900 UTC 25 June 1991.

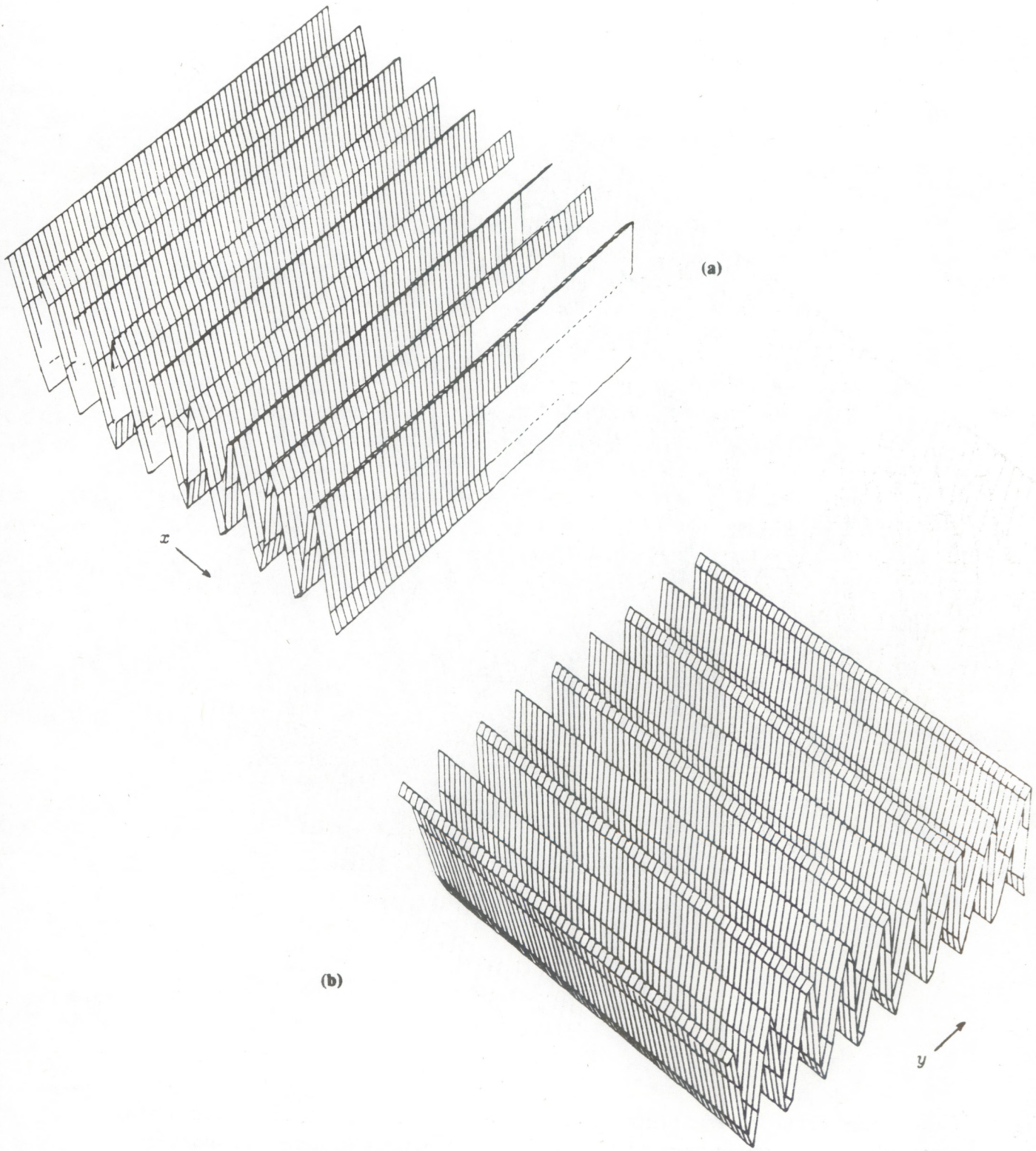

Fig 7. (a) Three-dimensional plot of standing waves used to represent background, and (b) its orthogonal counterpart used to represent GOES field. Both sets of waves are $2\pi/6.5$ gs^{-1} in wave number.

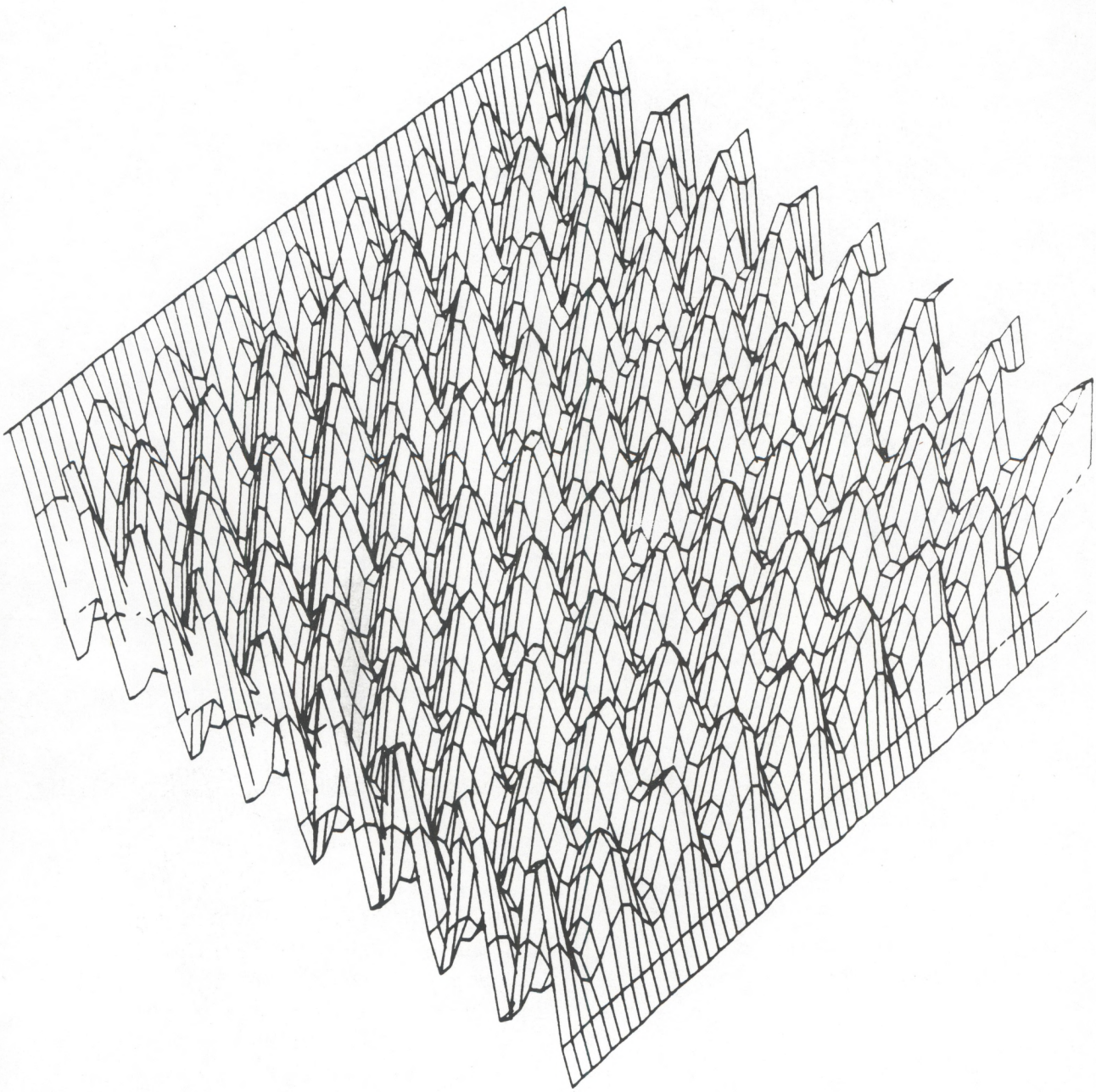

Fig. 8. Three-dimensional representation of solution generated by (A.8). Equation 8 was solved numerically using successive relaxation with approximately 70 iterations, converging to a normalized residual of 10^{-5}.

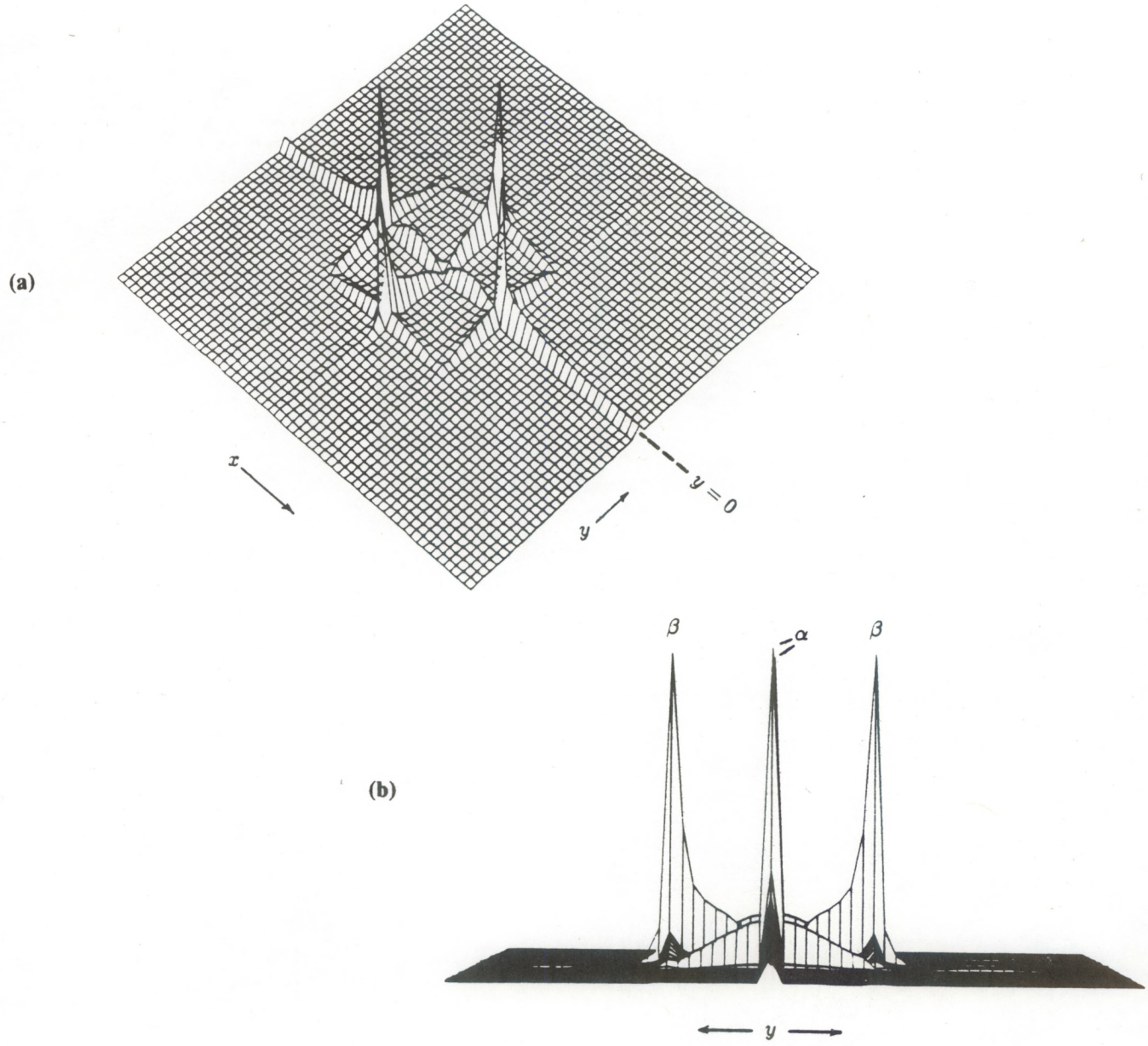

Fig. 9. Two views of three-dimensional representation of Fourier-transformed solution showing prominent amplitudes as a function of wave number. The resulting output was generated from two pure wave forms subjected to the analysis. (a) shows a view elevated about 45 degrees above the wave number plane. Each pair of peaks correspond to the waves in the orthogonal directions. The peaks aligned on the y-axis (y=0) represent the α term, the other pair result from the β (gradient) term. (b) shows the same surface but looks slightly above the plane with the observer oriented in line with the x-axis. The heights of the peaks are nearly the same indicating that the amplitude of each orthogonal wave in the solution was handled in roughly the same manner. Besides producing an analysis with equally balanced outputs, there is evidence of higher frequencies generated in the x-direction and lower frequencies generated in both the x- and y-directions. One explanation for these "artifacts" may be edge effects. Edges of the domain are not analyzed since the method of solution requires a boundary two elements deep resulting in slight discontinuities at edges. To avoid edge problems, one can analyze an area slightly larger than the desired domain.